Q-MAT+: An Error-Controllable and Feature-Sensitive Simplification Algorithm for Medial Axis Transform

YiLing Pan[a], Bin Wang[a,*], Xiaohu Guo[b], Hua Zeng[a], Yuexin Ma[c], Wenping Wang[c]

[a] *Tsinghua University*
[b] *University of Texas at Dallas*
[c] *University of Hong Kong*

Abstract

The medial axis transform (MAT), as an intrinsic shape representation, plays an important role in shape approximation, recognition and retrieval. Q-MAT is a state-of-the-art algorithm driven by quadratic error minimization to compute a geometrically precise, structurally concise, and compact representation of the MAT for 3D shapes. In this work we extend the technique to make it more robust, controllable, and name it *Q-MAT+*. Combining shape diameter function (SDF) and other mesh information, Q-MAT+ gets a more complete and accurate initial MAT than Q-MAT, even for extreme thin features, such as wires and sheets. Q-MAT+ could quickly remove insignificant branches while preserving significant ones to get a simple and faithful piecewise linear approximation of the MAT. Moreover, it performs the medial axis simplification with explicit maintenance and the control of Hausdorff error, which is not originally supported in Q-MAT. We further demonstrate the outstanding efficiency and accuracy of our method compared with other existing approaches for MAT generation and simplification.
Keywords: Medial Axis, Simplification, Error-Controllable

1. Introduction

The medial axis transform (MAT) is an intrinsic shape representation proposed by Blum (1967). Given a solid 3D object, the medial axis contains all the centers of the spheres which are called *medial spheres* inside the object while touching the boundary at two or more points. The MAT is composed of medial axis and the associated radius function that stores the distance to the boundary for each point on the medial axis. Due to its direct access to both the shape interior and the object's boundary, the MAT has been widely used in shape analysis, recognition, abstraction, and segmentation. There are already many methods to approximate the medial axis or the MAT. The most notable one is Amenta et al. (2001) that is based on the Voronoi diagram of a set of dense sample points on the object's boundary. To approximate the MAT of a 3D shape more accurately and compactly, *medial mesh* was introduced by Li et al. (2015); Sun et al. (2016) as a 2D simplicial complex embedded in 4D, which can also be regarded as a non-manifold triangle mesh consisting of vertices (*medial spheres*), line segments (called *medial cones*) and triangle faces (called *medial slabs*). Despite years of research and its potential utility, the wide spread of the application of MAT is still hindered by its redundancy and instability due to its high sensitivity to the boundary noise and variations. Even small perturbations to the object's boundary will bring plenty of unstable and redundant branches called *spikes* to the MAT. Q-MAT Li et al. (2015) is an efficient method to solve the above problems. It is inspired by both the Quadratic Error Metric (QEM) framework Garland (1997) for mesh decimation and Spherical QEM method Thiery et al. (2013), but is specifically designed for MAT simplification. To be more

*Corresponding author
Email addresses: pyl16@mails.tsinghua.edu.cn (YiLing Pan), wangbins@tsinghua.edu.cn (Bin Wang), xguo@utdallas.edu (Xiaohu Guo), zenghua16@mails.tsinghua.edu.cn (Hua Zeng), yuexinma@126.com (Yuexin Ma), wenping@cs.hku.hk (Wenping Wang)

specific, Q-MAT proposes a new quadratic error metric, called *slab quadratic error metric*, to measure the deviation from the original MAT, and a new *stability ratio* to identify the geometric significance of each edge of a medial mesh. The piecewise linear interpolation, instead of ordinary union, of the adjacent medial spheres can achieve both visual and numerical fidelity in approximating the input shape.

However, Q-MAT is still not a perfect solution. It includes two stages: the initialization which generates the medial mesh for an input shape, and the simplification which continuously decimates the medial mesh by an iterative edge-collapse strategy. For the former, it uses the original Voronoi vertices as medial vertices by the method Amenta et al. (2001) without "poles" filtering. Like many other existing approaches, this method is also difficult to approximate the media axis in the extremely flat or thin places of the object and then cause the MAT partially deleted. This problem is significant since without a complete initialized MAT, the following simplification process will undoubtedly exacerbate this inaccuracy and lead to a poor-quality MAT. Secondly, although Q-MAT introduces the stability ratio to distinguish the medial edges related to spikes at the early stage of simplification, it is still not feature-sensitive to preserve some geometrically insignificant (e.g. small Hausdorff error) but semantically important features, such as the tubular structure of many shapes. Thirdly, when an edge is collapsed in the simplifying operation, Q-MAT places a new medial sphere at either the place minimizing the quadratic function or the midpoint of the edge. Neither solution takes account of the situation that the new sphere is possible to be positioned outside the model, which violates the definition of the medial axis. Finally, as noted by Yan et al. (2016), Q-MAT lacks a general geometric metric (e.g. Hausdorff error) to help users control the simplification, which cannot be achieved by either the stability ratio or the slab quadratic error metric. The Hausdorff distance between the original shape and reconstructed shape by its medial mesh is an ideal choice, but evaluating the Hausdorff distance is a costly operation that will undermine the efficiency advantage of QEM framework.

Therefore, based on Q-MAT, we present Q-MAT+, which solves the above problems to make the computation more robust, feature-sensitive, and make the resulting MAT error-bounded. Different from other MAT generation methods requiring excessive number of samples to capture thin features while producing more redundant medial vertices, Q-MAT+ uses an automatic adaptive strategy to decide an appropriate amount of sampling points, and combines shape diameter function (SDF) Shapira et al. (2007) of surfaces and inscribed spheres to compute a structurally-complete medial mesh in the initialization. For the prevention of erroneous cases and the preservation of significant details, the edge-collapse strategy in Q-MAT is adjusted correspondingly. Furthermore, Q-MAT+ performs a local error update scheme to efficiently evaluate the one-sided Hausdorff distance so as to control the simplification process under a predefined threshold. In summary, we claim the following contributions:

- An adaptive MAT generation method to obtain the structurally-complete initial MAT even for a shape containing extremely thin features.
- An error-bounded simplification algorithm for MAT with the guarantee of accuracy at different levels and the protection of important detailed features.
- A complete method to obtain the geometrically correct, semantically complete, and compact MAT representation directly from an original shape.

The remainder of this article is organized as follows. Related works about MAT computation and simplification are discussed in Section 2. In Section 3 we briefly describe the medial mesh representation and Q-MAT as preliminaries, then carefully introduce our improvements from three aspects. The experiments in Section 4 validate and compare our algorithm with other start-of-the-art methods. Finally the conclusion and future work are presented in Section 5.

2. Related Works

2.1. MAT Computation Methods

For 2D smooth shapes, it has been proved that the Voronoi vertices of the samples on the shape's boundary topologically and geometrically converge to its medial axis Brandt and Algazi (1992). However,

the same argument does not hold in 3D cases due to the existence of "slivers", which are flat tetrahedra of small volume but do not have degenerate faces. The centers of circumscribing spheres (approximated Voronoi vertices) for such sliver tetrahedra are far away from medial axis. Consequently, for 3D shapes represented by triangle meshes, the most commonly-used method is to obtain sampling points on the surfaces and filter the Voronoi diagram of these samples or other derivative structures to get the approximation of medial axis. The most notably one is Amenta et al. (2001) which proposed the "poles filtering" to get a subset of Voronoi diagram approximating the medial axis as the sampling density increases. This method can be categorized into the *angle-based filtering methods* which also include approaches of Attali and Montanvert (1996); Dey and Zhao (2004). Generally speaking, these methods compute the angle formed by each medial vertices and its two closest points on the object's surface, then remove the medial vertex if the associated angle is less than a user-specified threshold. Although these methods have some advantages in retaining local features, they are usually difficult to preserve the topology of the input shape.

SAT Miklos et al. (2010) is a *scale-based medial axis transform method* which not only produces MAT in a numerically robust manner but also efficiently prunes spikes. It first scales all medial spheres by a factor $s > 1$, then removes those ones contained in other medial spheres. Not until all medial spheres are scaled by the factor $1/s$ is the final approximation result obtained. Since narrow gaps or small holes may disturb the scaling step, SAT has the same defect as the *angle-based filtering methods*. It can not control the level of simplification except for setting the value of scale.

λ-medial axis methods belong to another category using the circumradius of the closest points of a medial vertex as a filtering criterion. Typical algorithms like Pizer et al. (2003); Chazal and Lieutier (2005) discard a medial vertex if the circumradius is smaller than a given threshold λ. However, the result may lose some features, which are needed to be reserved.

Voxel-based methods, completely different from the above methods, require the shape to be represented by a union of voxels and select a subset sharing similar properties as medial axis, for example, being thin, centered and preserving the topology and components of shape Saha et al. (2016); Sobiecki et al. (2014). If the shape is not in voxel representation, it should be converted by voxelization first. These methods guided by non-Euclidean distance metrics like Manhattan distance Palgyi and Kuba (1999); Tsao and Fu (1981) or chamfer distance Pudney (1998) result in less accurate MAT than those that compute in Euclidean distance field Hesselink and Roerdink (2008); Rumpf and Telea (2002) or use more global shape information Jalba et al. (2016). The state-of-the-art method of this category is Voxel Core Yan et al. (2018), which is based on an observation that the interior Voronoi of the boundary vertices can faithfully approximate the medial axis of a voxel shape. Even so, there is a common disadvantage of these methods – the finer the voxel resolution is, the higher the computational cost required. Moreover, it is inevitable to increase resolution when pursuing geometric accuracy. Based on the essential difference from these voxel-based methods, all previously-discussed methods can be grouped together into the category of *sampling-based methods*.

2.2. MAT Simplification Methods

The progressive MAT (PMAT) method Faraj et al. (2013), improving the SAT, simplifies the transformation by collapsing the edges. For each edge connecting two medial spheres, the method calculates the ratio value of the distance between two centers to the difference between two radii of the two medial spheres. Using this ratio as the collapsing cost, it can simplify the MAT in an orderly and reasonable way. However, PMAT does not optimize the position of the new medial sphere after merging an edge in the simplification process, just simply choosing the center of the relatively large sphere.

An alternative method based on the idea of error-control is Hausdorff Error-based Method (HEM) Sun et al. (2016). When merging edges, HEM computes the one-sided Hausdorff distance from the original surface to the boundary of the shape reconstructed from the simplified medial mesh to control the approximation error. Although Hausdorff distance is a faithful measure of the approximation error, precisely computing the Hausdorff distance is prohibitively slow. After computing the error estimation for two endpoints of an edge, the one with smaller Hausdorff distance is selected as the new medial vertex. So similar to PMAT, it is still hard to obtain a superior medial sphere.

Compared with the above two methods, Q-MAT Li et al. (2015) proposes a new edge-collapse cost which can be quickly updated, and can effectively optimize the placement of new medial spheres. It adopts

quadratic error metric (QEM) Garland (1997) framework for edge collapse and proposes two novel metrics: the slab quadratic error (SQE) and stability ratio. For each medial sphere of the simplified medial mesh, SQE measures its "distance" to the incident slab of the initial medial mesh, and the stability ratio predicts how likely a medial edge is a spike. When merging an edge, the collapsing cost is defined as the sum of terms combining SQE and stability ratio of two end medial spheres. After getting an initial medial mesh, all the edges are queued based on their collapsing costs, then the edge with minimum cost is popped and collapsed to generate a new medial sphere. New edges are pushed into the queue according to their computed costs. The preservation of boundary and topology is also considered in the simplification. Due to the efficiency and superiority of Q-MAT, Lan et al. (2017) uses it to extract and simplify the MAT as the basis of their volume-preserving shape deformation algorithm, and Yang et al. (2018) extends this framework to get the Deformable MAT (DMAT) for animated mesh approximation.

Yan et al. (2016) introduced a popular global significance measurement named Erosion Thickness (ET) over the medial axis of 3D shapes, which is extended nicely from 2D. It extracts a curve subset guided by ET from the initial medial axis according to the observation that the curve skeleton in fact reveals the branching structure of the root, which plant biologists usually use to explain the root system architecture. In comparison, the ET method can create a greater variety of skeletons than Q-MAT due to its independent control of the 2D and 1D components. Guided by the local measurement only, Q-MAT is hard to interpret the pruning process. In this paper, we improve over Q-MAT by locally updating the one-sided Hausdorff error and distinguishing tubular shape feature to control the quality of MAT simplification.

3. Approach

3.1. Preliminaries

As preliminaries, we first briefly introduce the 3D medial mesh representation and review Q-MAT with its important formulas.

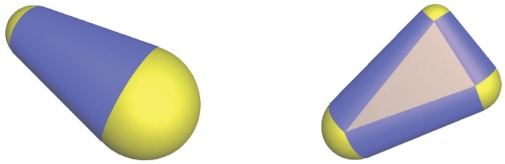

Figure 1: Interpolation of medial spheres Li et al. (2015). (a) Medial cone: the enveloping primitive of a medial edge. (b) Medial slab: the enveloping primitive of a medial face.

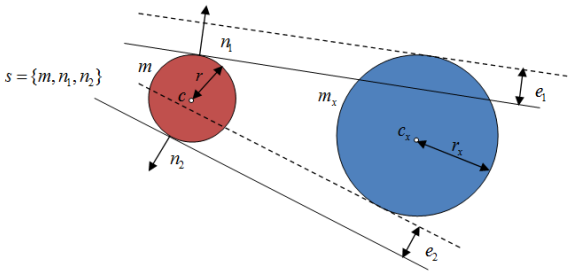

Figure 2: Description of SQE function Li et al. (2015). The sphere $\mathbf{m} = (\mathbf{c}^\top, r)^\top$ (in red) and two outward unit normal vectors $\mathbf{n}_1$, $\mathbf{n}_2$ of the bounding planes tangent to $\mathbf{m}$ define a slab. The SQE function measures the distance from a variable sphere $\mathbf{m}_x = (\mathbf{c}_x^\top, r_x)^\top$ (in blue) to the slab.

3.1.1. Medial Mesh Representation

We follow the medial mesh representation proposed by Li et al. (2015); Sun et al. (2016) for better volume representation and MAT approximation. A medial mesh M_s for a 3D shape S is a 2D simplicial complex which is embedded in $\mathbb{R}^4$ to approximate the shape's MAT. A medial mesh is composed of vertices, edges, and triangle faces. Each vertex $\mathbf{m}_i$ in M_s is called a medial vertex and represents a medial sphere, denoted as a 4D point $\mathbf{m} = (\mathbf{c}^\top, r)^\top$, where $\mathbf{c} \in \mathbb{R}^3$ is the position of the vertex and r is its associated radius. The edge of the medial mesh is called the medial edge and given by $e_{ij} = \{\mathbf{m}_i, \mathbf{m}_j\}$, represented by $(1-t)\mathbf{m}_i + t\mathbf{m}_j, t \in [0,1]$, a convex interpolation of its incident two endpoints $\mathbf{m}_i$ and $\mathbf{m}_j$. Likewise, a triangle

face of the mesh is called a medial face and denoted as $f_{ijk} = \{\mathbf{m}_i, \mathbf{m}_j, \mathbf{m}_k\}$, represented by the convex combination of three medial spheres, $a_1\mathbf{m}_i + a_2\mathbf{m}_j + a_3\mathbf{m}_k$, with $a_i (i = 1, 2, 3) \geq 0$ and $a_1 + a_2 + a_3 = 1$. Each discrete component mentioned above corresponds to a volume primitive: a medial vertex being a medial sphere, a medial edge being a medial cone which comprises two spherical caps connected by a truncated cone, and a medial face being a medial slab which is the convex hull of three medial spheres as shown in Figure 1. After piecewise linear interpolation, the 3D shape represented by the enveloping volume of the medial mesh is more accurately and compactly than merely using the union of medial spheres.

3.1.2. Q-MAT

Q-MAT is an efficient method to obtain a structurally simple, compact and accurate linear approximation of MAT by edge contraction. The simplification process is guided by the collapse cost which combines two novel metrics: the slab quadratic error (SQE), and the stability ratio. We will briefly introduce the definitions of these functions.

Figure 2 shows an intuitive description of SQE. Suppose for a common sphere is $\mathbf{m} = (\mathbf{c}^\top, r)^\top$ (in red), an extended slab s is defined as its two tangent planes and denoted by $s = \{\mathbf{m}, \mathbf{n}_1, \mathbf{n}_2\}$, where $\mathbf{n}_1$ and $\mathbf{n}_2$ are the outward unit normal vectors of the planes, as shown in Figure 2. Let us denote $\overline{\mathbf{n}}_1 = (\mathbf{n}_1^\top, 1)^\top$ and $\overline{\mathbf{n}}_2 = (\mathbf{n}_2^\top, 1)^\top$. For the variable sphere $\mathbf{m}_x = (\mathbf{c}_x^\top, r_x)^\top$ (in blue), Q-MAT defines the $SQE_s(\mathbf{m}_x)$, that is slab quadratic error measuring the squared distance from sphere $\mathbf{m}_x$ to the slab s:

$$SQE_s(\mathbf{m}_x) = \mathbf{m}_x^\top \cdot \mathbf{A} \cdot \mathbf{m}_x + \mathbf{b}^\top \cdot \mathbf{m}_x + c, \tag{1}$$

where

$$\begin{aligned} \mathbf{A} &= \overline{\mathbf{n}}_1 \cdot \overline{\mathbf{n}}_1^\top + \overline{\mathbf{n}}_2 \cdot \overline{\mathbf{n}}_2^\top, \\ \mathbf{b} &= -2\mathbf{A} \cdot \mathbf{m}, \\ c &= \mathbf{m}^\top \cdot \mathbf{A} \cdot \mathbf{m}. \end{aligned} \tag{2}$$

When an edge $e_{ij} = (\mathbf{m}_i, \mathbf{m}_j)$ is collapsed, the optimal new sphere $\mathbf{m}_g$ becomes associated with all the slabs of two medial spheres $\mathbf{m}_i$ and $\mathbf{m}_j$. It can be computed by minimizing the quadratic function:

$$E^e_{\mathbf{m}_i,\mathbf{m}_j}(\mathbf{m}_x) = \mathbf{m}_x^\top \cdot \mathbf{A}_{\mathbf{m}_g} \cdot \mathbf{m}_x + \mathbf{b}_{\mathbf{m}_g}^\top \cdot \mathbf{m}_x + c_{\mathbf{m}_g}, \tag{3}$$

which is equal to the sum of SQE of $\mathbf{m}_g$ with all associated slabs $slabs(\mathbf{m}_g) = slabs(\mathbf{m}_i) \cup slabs(\mathbf{m}_j)$.

The hyperbolic distance between two medial spheres is defined as:

$$d_h(\mathbf{m}_i, \mathbf{m}_j) = max\{0, \|\mathbf{c}_i - \mathbf{c}_j\| - |r_i - r_j|\}. \tag{4}$$

Then another important metric of this edge, *stability ratio*, is defined as the ratio of this hyperbolic distance to the edge length:

$$\Gamma_{ij} = \frac{d_h(\mathbf{m}_i, \mathbf{m}_j)}{\|\mathbf{c}_i - \mathbf{c}_j\|}, \tag{5}$$

where Γ_{ij} represents the stability of this edge, or how likely it is not a spike. In particular, when Γ_{ij} is 0 for two independent spheres $\mathbf{m}_i$ and $\mathbf{m}_j$, the smaller sphere is contained inside the larger one, then the edge is a pure spike; when Γ_{ij} is 1, the radii are equal and the edge is completely stable and geometric significant. Finally the collapse cost for this edge is defined as:

$$c_{ij} = (E^e_{\mathbf{m}_i,\mathbf{m}_j}(\mathbf{m}_g) + k) * \Gamma_{ij}^2, \tag{6}$$

where k is positive constant. Q-MAT follows the QEM framework to queue all edges in the medial mesh according to their cost values c_{ij}, and iteratively collapses the edge with minimum cost to generate a new medial sphere until the mesh is simplified to the specified number of medial vertices.

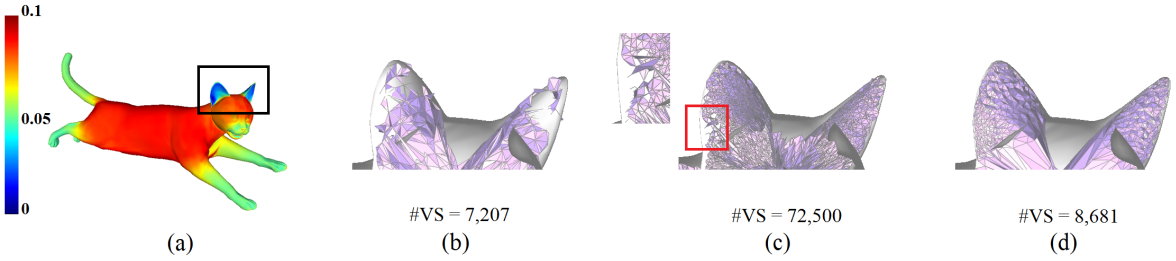

Figure 3: Comparing our method with a typical Voronoi-based method, the Power Crust (PC) Amenta et al. (2001) on an extremely thin sheet, Cat's ear. "#VS" is the number of sampling points in the input shape. (a) The color-coded distribution of SDF information for the whole Cat model (All the models in our experiments are scaled so that the diagonal length of their bounding boxes are equal to 1). The red parts are thicker, while the blue parts are thinner. (b) Initial MAT by PC from the original sampling points. (c) Initial MAT by PC from ten times of uniformly sampled points. (d) Initial MAT by Q-MAT+ from our adaptive sampling points.

3.2. Adaptive Initialization

Our method, named *Q-MAT+*, starts from computing an initial medial mesh for an input 3D shape. Note that for a typical thin feature, such as the Cat's ear in Figure 3(a), the original PC algorithm would produce a poor result without providing more sampling points, as shown in Figure 3(b). However, even if ten times of uniformly sampled points are given, it still generates a defective MAT with holes as shown in Figure3(c). Hence we propose a novel adaptive generation method, which needs only a little more sampling points and uses the centers of inscribed spheres to approximate medial vertices to obtain a more complete MAT even in extremely thin parts like Figure 3(d). It has two main steps: sampling and selecting those Voronoi vertices meeting our requirements from the Delaunay Triangulation of sampling points.

Firstly, instead of sampling uniformly on the whole surface, we found that uniformly sampling per triangle facet can get better results while reducing redundancy. To estimate the thickness of each facet, we use the shape diameter function (SDF) Shapira et al. (2007). For a closed manifold surface, SDF is a scalar function measuring the neighborhood diameter at each point and able to capture the object's volumetric shape locally. Q-MAT+ increases sampling points on those facets with large area or in thin patches by adding a slight local smoothing of sampling density:

$$n(f_i) = max\{0, \left\lceil \frac{A_i}{\min\limits_{f_j \in N(f_i)} A_j} \right\rceil - 1\} + n_f * TF(f_i), \tag{7}$$

where $n(f_i)$ is the increased number of sampling points of facet f_i, A_i is the area of f_i, $N(f_i)$ is the set of neighbour facets sharing vertices with f_i, and n_f is the average number of samples per facet located in thin patch. Choosing a large n_f offers more sampling points and a tighter approximation of surface, however, bringing more spikes and higher redundancy. In our experiments, we found $n_f = 1$ is enough to give a good trade-off between correctness and efficiency. $TF(fi)$ is an indicator function that determines whether the facet should be sampled with more points because of its thinness and can be expressed as:

$$TF(f_i) = \begin{cases} 0 & \text{if } SDF(f_i) > \theta \\ 1 & \text{if } SDF(f_i) \leq \theta, \end{cases} \tag{8}$$

where θ is an SDF threshold which is set as half of the average SDF value in our experiments. Certainly, θ is an important parameter affecting the behavior of the generation algorithm. We test many models to observe the influence of θ and choose a default setting. Figure 4 shows the approximation error influenced by

θ of three input models with extremely thin parts (Cat, Airplane and Fish) and two common input models (Bear and Dolphin). It is obvious that increasing the sampling according to the thickness can improve the results of initial medial mesh generation. We can see $\theta = 0.5 * average\_SDF$ is sufficient for most extreme cases, because choosing a larger value would cause unnecessary redundancy. Users could also adjust this parameter according to their own needs. We first randomly generate $n(f_i)$ samples on the triangle f_i, then perform a Lloyd relaxation process onto a Bounded Voronoi Diagram (BVD) Tournois et al. (2010). We find that five iterations are usually enough to obtain a quasi-uniform sampling on facets.

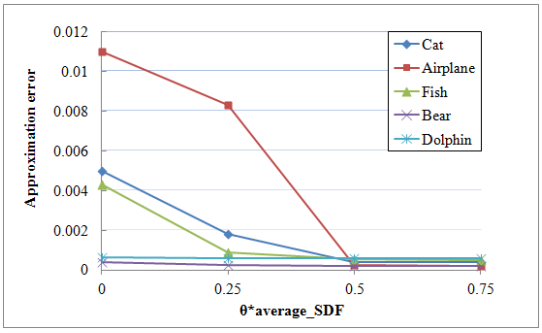

Figure 4: Influence of the SDF threshold θ. Its values are based on the average SDF values of respective models. When θ becomes bigger, the approximation error is smaller. At the same time, more redundancy will appear. It is obvious that 0.5 can make a better balance than others.

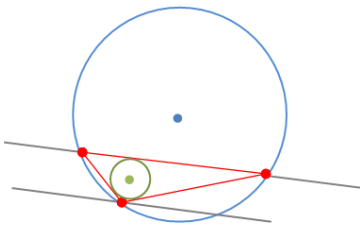

Figure 5: A 2D illustration for the defect of using circumcenter in thin parts. For a simplex with three sample points (red) lying in the thin parts (grey), their circumcenter (blue) is outside the model and the circumsphere (blue) is much larger than this part. Without very dense sampling, a better choice is the inscribed circle (green) in this case.

After obtaining enough sampling points, we use 3D Constrained Delaunay Triangulation and delete the outside tetrahedrons. That is, for each simplex of the Delaunay triangulation, which is a tetrahedron in 3D, if the center of its circumscribe sphere is inside the model, it is selected as a medial vertex since such approximation is precise enough in normal parts Amenta et al. (2001). Otherwise, we consider another case that the SDF values of all four vertices in this simplex are below θ. Considering an extreme case where the four points are almost co-planar but non-degenerate, their circumcenter is no longer in conformity with the requirements, resulting in the absence of a medial vertex here (see the 2D example in Figure 5). That is why there are holes in Figure 3(c). Hence for such tetrahedron, if the center of its inscribed sphere is inside the model, we take this center as medial vertex and the shortest distance from the center to the original surface as radius to form a medial sphere. This is a fast approximation method based on the assumption that the selected centers of inscribed spheres contain the correct medial vertices and the rest would be pruned off as spikes by Q-MAT+, which can be validated by the simplified medial mesh in our experiments. The procedure of selection is shown as Algorithm 1.

Finally, the connectivity among selected vertices is inherited from the simplices in triangulation to form a 2D non-manifold mesh. In this way, we get the initial medial mesh, which is noisy, dense, but geometrically complete to represent the medial axis of the input 3D shape.

3.3. Local Update of Hausdorff Distance

Q-MAT progressively performs edge contraction governed by the collapse cost to efficiently simplify the medial mesh. Although it can control the simplification by specifying the number of simplified medial vertices or the sum of collapse cost, neither of them is a general geometric metric to measure the approximation error-bound. While it is natural to think of taking the Hausdorff distance between the input shape and the shape reconstructed by simplified medial mesh as the measurement, the costly computation makes this idea impractical.

Note that HEM Sun et al. (2016) has argued that the one-sided Hausdorff distance from the boundary surface of the original shape to the boundary surface of reconstruction shape could provide a good approximation to the true Hausdorff distance if the medial mesh well approximates the original object. However,

Algorithm 1 Filtering Simplices in Delaunay Triangulation

Require: Simplex x, Input shape S
p = Circumcenter(x)
if InsideModel(p,S) **then**
    select p as medial vertex
    r = Circumcenter(x).radius
else
    q = Inscribedcenter(x)
    if ThinPart(x) and InsideModel (q,S) **then**
        select q as medial vertex
        r = ShortestDist(q,S)
    end if
end if

the one-sided Hausdorff distance computation is still time-consuming. In order to evaluate the one-sided Hausdorff distance in each edge-collapse operation to control the simplification under a user-specified threshold while maintaining the efficiency of Q-MAT, we use a rapid yet sufficiently accurate approximation of the distance. It is inspired by the surface remeshing method of Hu et al. (2017) by a local update scheme of the shortest links from medial vertices to surface in combination with previous careful surface sampling.

Suppose that M_s is the medial mesh for 3D shape S, $R(M_s)$ is the reconstructed shape through piecewise linear interpolation from M_s to approximate S. The one-sided Hausdorff distance from the boundary surface of the input S to the boundary surface of the approximation shape can be denoted as:

$$d_H(S, R(M_s)) = \max_{p \in S} d(p, R(M_s)), \tag{9}$$

with $d(p, R(M_s))$ being the minimal distance of a sample point p in the input surface to the reconstructed surface:

$$d(p, R(M_s)) = \min_{q \in M_s} d(p, R(q)), \tag{10}$$

where $R(q)$ is the set of volume primitives associated with medial vertex q.

We observe that each edge-collapse operation usually results in a greater Hausdorff distance and only changes a local region in the input surface in terms of its shortest distance to the enveloping volume represented by medial mesh. Hence it is possible to take a local update scheme to rapidly compute the one-sided Hausdorff distance as long as we decompose the input surface and medial mesh correctly. To be more specific, Q-MAT+ maintains a set of boundary points which we call *responsible region* for each medial vertex. This relationship starts with the four surface sampling points of the simplex and the corresponding medial vertex when generating the initial medial mesh (The center of the inscribed sphere of each simplex is a medial vertex, and it is responsible to the found nearest boundary points). This can be expressed as

$$Res(q) = \{p | p \in S, d(p, R(q)) = d(p, R(M_s))\}. \tag{11}$$

In other words, $Res(q)$ contains the closest boundary points on the input shape for q. When an edge is collapsed, the merged sphere inherits the responsible regions from the two medial spheres connected by this edge. Figure 6 shows a simple example.

Now we define C as a set of all medial vertices adjacent to this collapsed edge including the medial vertices at the endpoints and others adjacent to these two vertices, so the $\overline{C}$ is the vertices not affected by this edge. Then the input shape S can be decomposed to $S = S_C \cup S_{\overline{C}}$ as the responsible regions of C and $\overline{C}$ respectively. During the simplification, we have

$$d_H(S, M_s) \leq \max\{d_H(S_C, C), d_H(S_{\overline{C}}, \overline{C})\}, \tag{12}$$

to locally but efficiently approximate the one-sided Hausdorff distance because the $d_H(S_{\overline{C}}, \overline{C})$ is unchanged indeed. Consequently Q-MAT+ could rapidly evaluate the ones-sided Hausdorff distance to control the

simplification, by stopping the edge contraction when the resulting $d_H(S, M_s)$ is above a threshold, while still adopting the QEM framework for efficient maintenance of the quadratic error terms and error minimization.

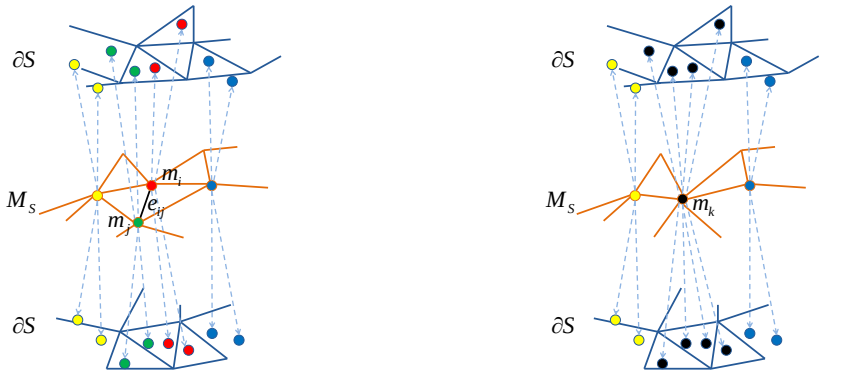

(a) Before edge e_{ij} is collapsed to m_k (b) After edge e_{ij} is collapsed to m_k

Figure 6: Inheritance of responsible regions during an edge-collapse operation. Each medial vertex in medial mesh (orange) has its responsible samples in the surface (blue). The change of sample color symbolizes the change of corresponding medial vertex and the dotted line represents the responsibility relationship.

3.4. Feature Sensitive Simplification

At the later stage of simplification, the medial edges corresponding to some geometrically insignificant (e.g. small Hausdorff error) but semantically important tubular structures (e.g. human fingers or octopus tentacles) would be collapsed for its collapse cost is relatively smaller than the other parts of the medial mesh. However, it is difficult to distinguish and protect these medial edges accurately. At the same time, users may prefer different features (plate-likeness or tubular shape parts) to be preserved in MAT simplifications. In this work, Q-MAT+ utilizes the maintained responsible relationship and just adds a mark for medial edges and medial vertices to solve the above problems.

The medial edges without adjacent faces are usually associated with the tubular structure but it is not true for all of them. In order to identify those medial edges associated with thin features, choosing a reference criterion is critical. In this work, we use the SDF values of medial vertices' responsible regions. Q-MAT+ distinguishes the medial edges that need to be protected by estimating whether the SDF values of its responsible regions are all below θ and without adjacent faces. The results are shown in Figure 7. As shown in Figure 7(c), the medial edges related to the head of Octopus are not selected as the target ones, since the SDF value of the associated responsible region is relatively large. The selected medial edges are marked as non-collapsible, and the medial vertices at endpoints are marked as non-merged, which means their spheres always serve as the new medial spheres when the other connected edges are collapsed. In this way, these significant medial edges could be preserved. It is worth mentioning that this strategy works at a later stage of simplification to prevent spikes from mistakenly being protected. When users intend to retain the tubular shape parts at any time of simplification, Q-MAT+ triggers the feature-preservation strategy by marking the selected medial edges as non-collapsible to achieve the goal. In this way, Q-MAT+ is able to create a greater variety of MAT representation than before.

In addition, we make Q-MAT+ more robust with additional boundary constraints. Note that for a medial edge $e_{ij} = \mathbf{m}_i, \mathbf{m}_j$ to be collapsed, if $\mathbf{A}$ in Equation 3 is invertible, Q-MAT computes the optimal sphere, otherwise it selects the sphere with the minimum $E^e_{\mathbf{m}_i,\mathbf{m}_j}(\mathbf{m}_x)$ from the three spheres: $\mathbf{m}_i$, $\mathbf{m}_j$, and $(\mathbf{m}_i + \mathbf{m}_j)/2$. There exists a possible error that the new medial sphere and its connected edges could be outside the model. To avoid this situation, Q-MAT+ modifies the selection of new medial spheres. That is, if $\mathbf{A}$ is not invertible or the computed optimal sphere has the above error (for simplicity, we just check whether the position of the new sphere and the midpoint of its connected edge is inside the model), Q-MAT+ chooses

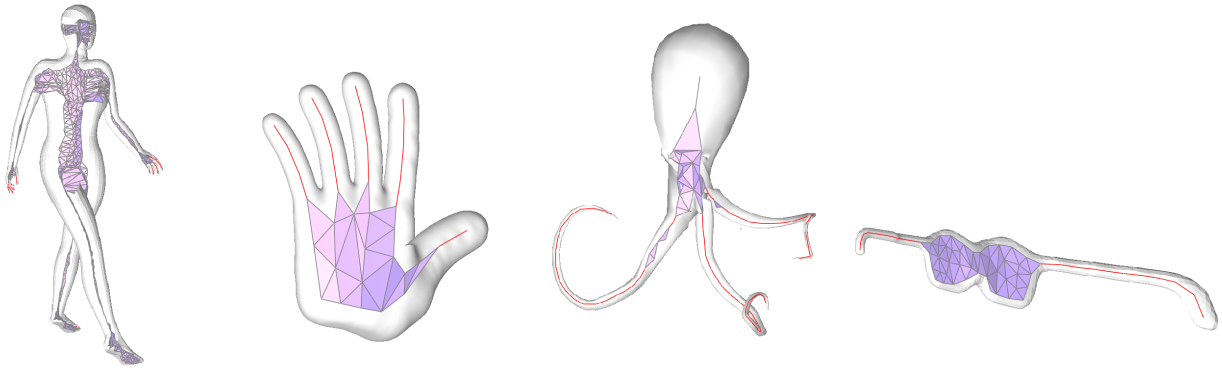

Figure 7: Feature recognition in Q-MAT+. #v is the number of medial vertices and ε is the approximation error. Models have been simplified to allow for more intuitive comparisons between medial edges. Red lines represent the medial edges associated with important tubular features and they would be protected in the following simplification.

the candidate out of $\mathbf{m}_i$, $\mathbf{m}_j$, and $(\mathbf{m}_i + \mathbf{m}_j)/2$ by: (1) minimizing $E^e_{\mathbf{m}_i,\mathbf{m}_j}(\mathbf{m}_x)$; and (2) guaranteeing the correctness mentioned above. If none of the four spheres meets both requirements, the edges are marked as non-collapsible.

It can be expected that when all medial edges are marked as non-collapsible, the medial mesh will not be further simplified.

4. Experimental Results

In this section we will show the computation and simplification results of Q-MAT+ for validation and comparisons with other methods. Q-MAT+ is implemented in C++ and the program runs on a Windows 7 workstation with an Intel i5 CPU @3.20GHz and 16 GB memory. All the processed models have been scaled to make the diagonal lengths of their bounding boxes equal to 1.

4.1. Computation of Initial MAT

Firstly we will show the initial MAT produced by our improved Voronoi-based method. We use the CGAL package "Delaunay Triangulation 3" to get the Delaunay Triangulation of the sample points and take its dual to get the Voronoi diagram. Besides, the package "Triangulated Surface Mesh Segmentation" provides a rapid calculation of SDF. Finally the CGAL package "Skin Mesh Generation" performs the conversion from a set of individual medial spheres into a triangle mesh representation of the MAT. To estimate the approximation accuracy of initial MAT, we use the one-sided Hausdorff distance from the input surface to the reconstructed surface, denoted as ε. Definition of ε is mentioned in the Section 3.3. The reconstructed model is the combination of all rendered primitives including medial spheres, medial cones, and medial slabs, so the ε can be computed by choosing the shortest distance from a point in the boundary surface of the input shape to all primitives with the greatest value.

We compare our approximation method with the following state-of-the-art methods which have publicly available executable programs: two sampling-based methods, the Power Crust (PC) Amenta et al. (2001) and the SAT Miklos et al. (2010), and a voxel-based method – the Voxel Core (VC) Yan et al. (2018). The former two are the generation methods used by Q-MAT. Since all these methods have pruning process, we add our results simplified by Q-MAT+ to the same number of vertices as PC. In addition to the commonly used evaluation metric ε, we also show our qualitative results to give a visual comparison in Figure 8 and demonstrate how our approach outperforms the others.

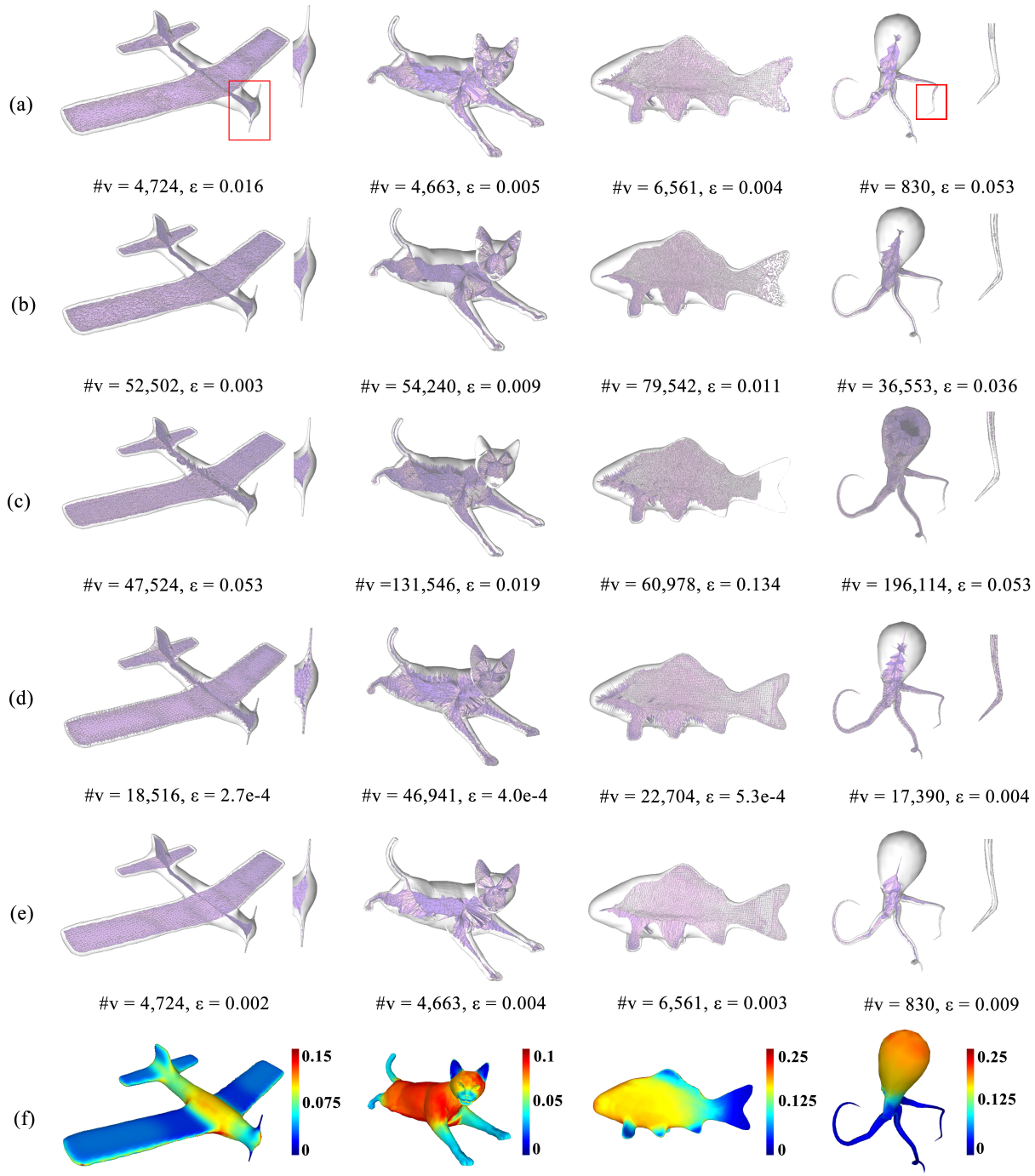

Figure 8: The comparison of initialization results between our Q-MAT+ and other methods. #v is the number of medial spheres, and ε is the approximation error. (a) The results by PC. (b) The results by SAT. Q-MAT usually takes the results of PC or SAT as initial medial mesh. (c) The results by VC. (d) The results by Q-MAT+, and (e) is the simplified medial mesh by Q-MAT+ in order to compare with the based method PC. (f) The color-coded distribution of SDF information for each model, red denotes thicker, while blue denotes thinner.

Model(#VS)	PC(s)	SAT(s)	VC(s)	Our method(s)
Airplane(5,631)	3.0	52.5	7.0	3.7
Cat(7,207)	3.2	67.5	50.7	6.5
Fish(6,833)	3.8	92.9	11.7	5.0
Octopus(1,343)	1.3	62.0	17.1	1.8

Table 1: "#VS" is the number of vertices in the input shape. The first column shows model, and the other columns show the timing used by different methods to generate initial medial mesh. Note that we do not count the time spent on voxelization for the VC method.

Model(#VM)	HEM	Q-MAT+	Ratio of time
Glasses(6,663)	39.9s/42	3.8s/27	10.5
Ant(19,664)	100.9s/75	9.7s/66	10.4
Chair(27,257)	287.7s/83	14.1s/61	20.4
Hand(41,247)	429.8s/64	20.6s/59	20.9
Table(42,266)	568.7s/120	20.0s/112	28.4

Table 2: "#VM" is the number of vertices in the initial medial mesh. The second and third columns show the simplification time and the number of vertices of HEM and Q-MAT+, and the fourth column shows the ratios of simplification time of HEM over to that of Q-MAT+. All the models are simplified until the approximation error is 0.01.

Comparison with the PC method. For PC, we use the default setting in which the sampling density constant is set as 0.6 and the parameter deciding whether to propagate the same label ("inside" or "outside") to neighboring poles is set as 0.4. Furthermore, the implementation of PC we used is in the VTK environment, it runs faster than any other versions. As a relatively early method, PC is widely used for its strong scalability and efficiency by the use of boundary samples. However, from the other hand, the reliance on surface sampling points makes it difficult to guarantee the robustness and correctness like the outliers in the tail of Fish model and ears of Cat model in Figure 8(a). As explained in Section 3.2, the circumscribing spheres to approximate Voronoi diagram aggravate the loss of details, which can be seen in tentacles of Octopus model and other thin tubular or sheet structures in other models. On the contrary, our Q-MAT+ inherits its advantages while maintaining these features completely.

Comparison with the SAT method. For SAT, we set the sampling distance to the default value, which is 0.01, and the scaling parameter to $s = 1.1$. SAT spends much time in converting the input mesh to a union of balls and the implementation focuses more on robustness rather than the speed. Hence SAT is always the most time-consuming one in sampling-based methods, which can be seen in Table 1. Compared with PC, SAT does not produce so many outliers, but it unfortunately could not guarantee the connections for thin features of MAT on the shapes unless given vast sample points. As shown in Figure 8(b), the medial mesh generated by SAT are much more redundant than PC and our Q-MAT+.

Comparison with the VC method. Because the input shape is represented by mesh, we first use Polymender Ju (2004) to perform the voxelization. We set the depth of octree to 9 so that the volume has an effective resolution of 512 in each X, Y, Z direction and the size of the model relative to the size of the bounding box of the volume grid is set to 0.9. Then the VC approximates medial axis from volume with setting the pruning parameter λ to 0.015 (for octopus which have more extremely thin features we set it to 0.005 to preserve more details) to filter those voxel cores whose radius value is less than λ. In this way, VC can get a good enough geometric approximation to the medial axis under normal circumstances. However, quite different from other methods, VC generates the approximation of medial axes from interior voxels of shape, leading to a certain deletion of the boundary information. In addition, VC produces extremely large number of medial vertices and edges which makes it inapplicable for the input of our simplified algorithm, considering that the computation time of Q-MAT is directly proportional to the number of medial edges. According to the design of VC algorithm, the smaller the λ value, the more the number of medial axis points retained. However, even when λ is equal to 0.005 such a low value cannot maintain the flat or minute geometric features. Compared with the Voxel Core, we would like to claim that the importance of topological

artifacts represented by Euler characteristic is far less than that of capturing complete geometric features of model.

Previous sampling-based methods always need excessive samples to capture thin features, however, our adaptive sampling and selective integration of the inscribed sphere scheme make Q-MAT+ no longer trapped in such a dilemma. In essence, Q-MAT+ can capture the most complete details with less points in a relatively short time.

4.2. Error-bounded Simplification

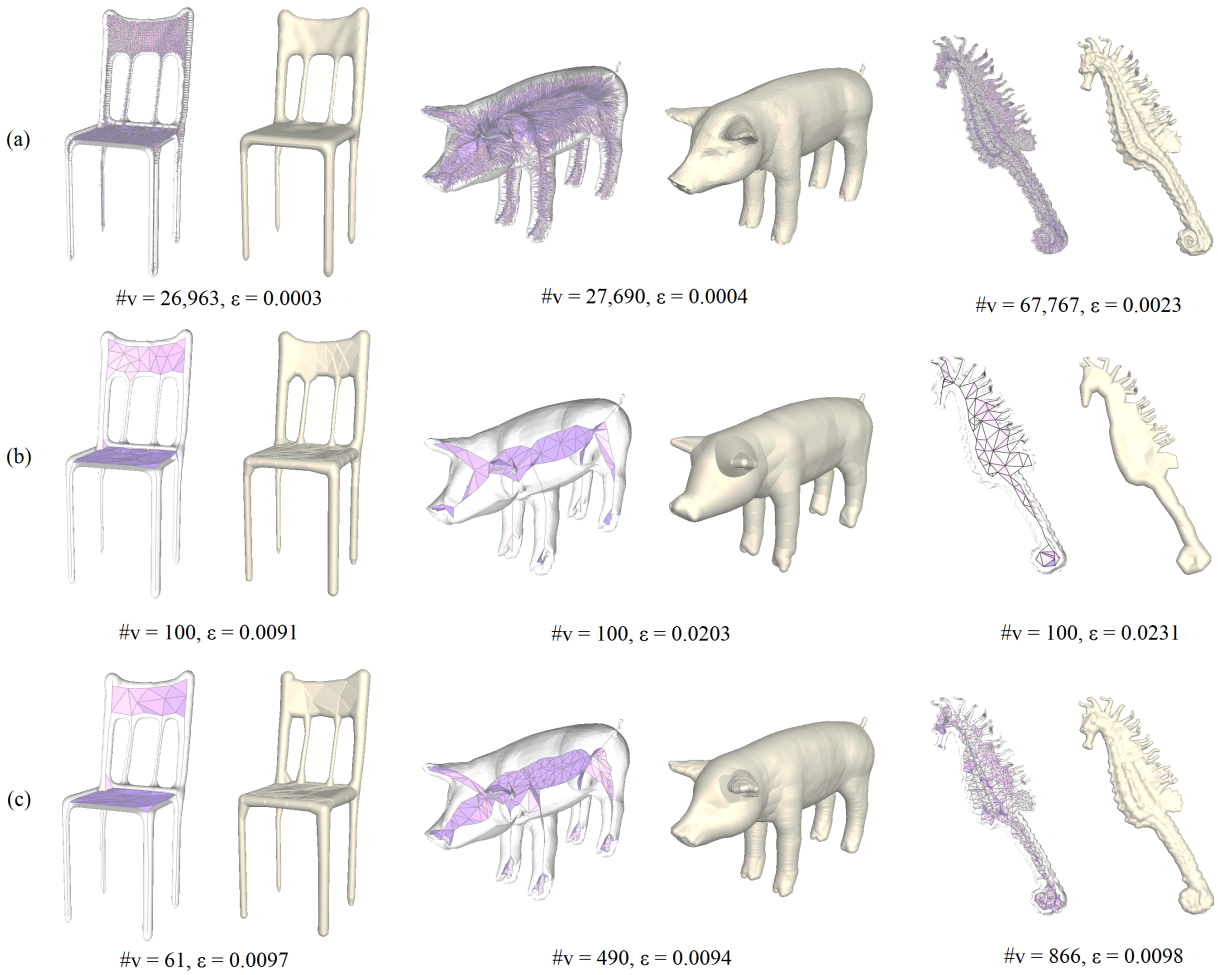

Figure 9: The comparisons of simplifications controlled by a user-specified number of medial vertices (Q-MAT) with a user-specified threshold of one-sided Hausdorff distance (Q-MAT+). (a) The initial medial meshes and input surfaces of Chair, Pig, and Seahorse models. (b) The simplified medial meshes by setting the number of medial vertices #v = 100 and their reconstructed models by Q-MAT. Q-MAT only provides this way to control simplification, however it is not universal. (c) The simplified medial meshes by setting the distance threshold to 0.01 and their reconstructed models by Q-MAT+.

In Q-MAT, users could stop the simplification by setting either a threshold of the sum of collapse cost, or the number of remaining medial vertices. For the former, it is a combination of the local significance measure (stability ratio) and heuristically defined error metric (SQE) without global geometric error-bound. For the latter, it cannot be used to control the simplification uniformly. As shown in Figure 9(b), 100 medial vertices are sufficient to approximate the original model for the Chair model, while for the Pig and Seahorse

models it causes many details lost and leads to greater errors, even though the former two models have similar number of initial medial vertices. By contrast, Q-MAT+ rapidly estimates the one-sided Hausdorff distance after each edge collapse to help users control the simplification with intuitive geometric meaning. In Figure 9(c), different models have different number of medial vertices, but have the nearly same distance threshold 0.01. Compared with the state-of-the-art simplification method HEM Sun et al. (2016) which is directly guided by one-sided Hausdorff error metric, Q-MAT+ uses much less time to simplify medial meshes near the specified threshold because of the advantages of local update and the efficiency of quadratic error minimization. Table 2 gives the simplification time of Q-MAT+ and HEM from the initial medial meshes of various objects to the simplified medial meshes with ε under 0.01. As shown in Table 2, HEM takes at least 10 times as much time as Q-MAT+ for the same error threshold. The superiority of Q-MAT+ will become more and more obvious with the number of initial medial vertices increasing. By carefully choosing the position of the merged medial sphere after edge collapse with feature preservation, Q-MAT+ gets similar concise results with HEM under this threshold. We show more simplification results controlled by different one-sided Hausdorff distance thresholds and their computation time in supplementary materials.

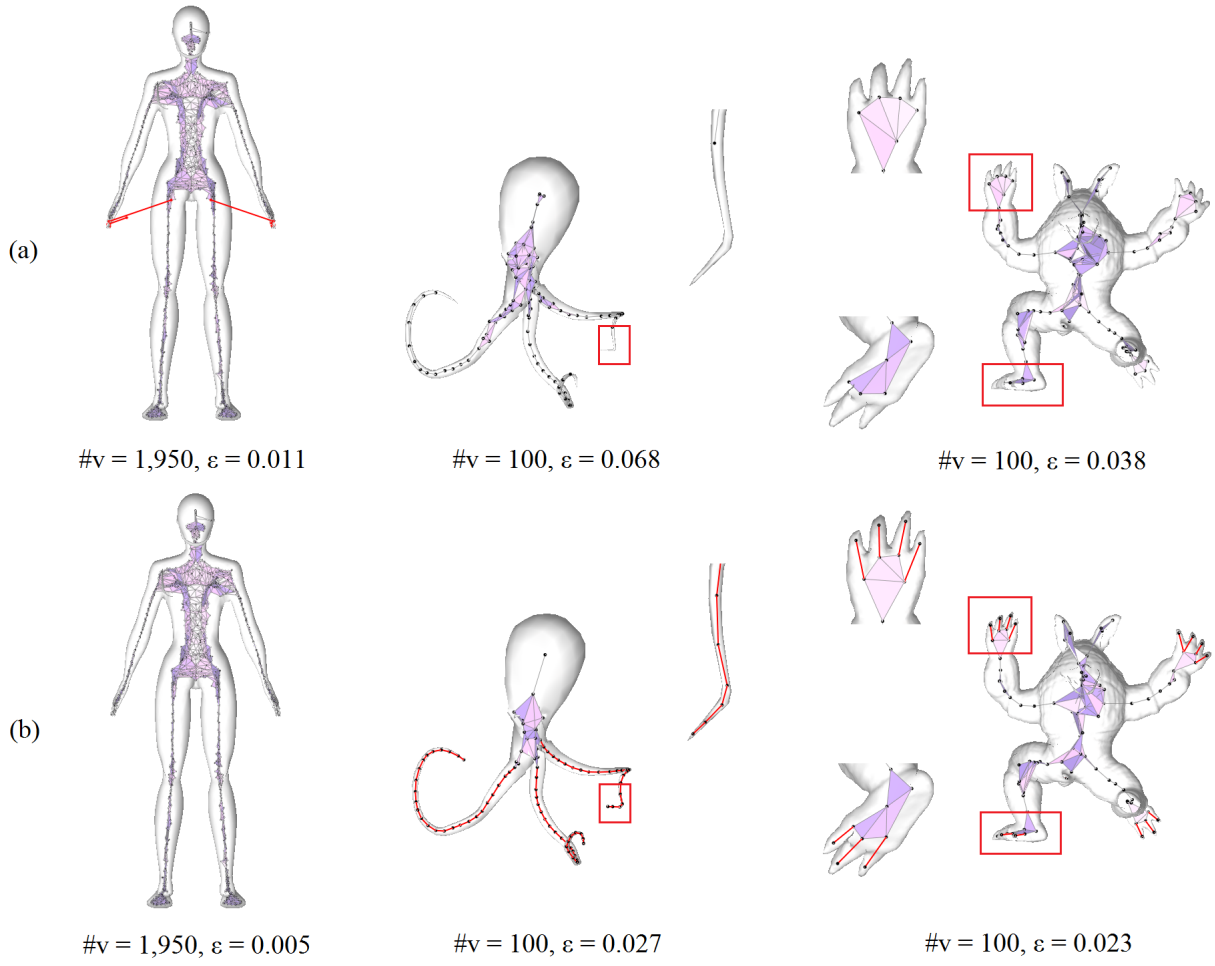

Figure 10: More comparisons with Q-MAT. (a) The results of Q-MAT. (b) The results of Q-MAT+. For the Man model (first column) Q-MAT produces a wrong simplification result in which some medial vertices and edges (red) are outside the model. Q-MAT+ outputs correct results. For the Octopus and Armadillo models (second and third column), Q-MAT cannot protect some important tubular structures like tentacles and fingers during the simplification. With feature recognition and protection of important medial edges (red), Q-MAT+ can preserve these structures.

In addition to initialization and error-bounded simplification, Q-MAT+ has made other improvements over Q-MAT. The Woman model in Figure 10(a) shows an error result of Q-MAT when it is simplified to 1950 vertices. This is caused by the fact that the merged medial sphere computed as the minimizer of collapse cost function does not consider the boundary constraints. Q-MAT+ considers this situation and improves it as shown in Figure 10(b). Moreover, at a later stage of simplification, the results of Q-MAT may lose important details like the tentacles of Octopus and toe fingers of Armadillo model with only 100 medial vertices in Figure 10(a), while Q-MAT+ is feature sensitive enough to preserve this information, which can be demonstrated by the red medial edges identified and protected as shown in Figure 10(b).

5. Conclusion and Future Work

We have presented an enhanced version of Q-MAT, called Q-MAT+, which is error-controllable and feature-sensitive for the simplification of MAT. Compared with PC and SAT which are used to generate initial medial mesh by Q-MAT, we combine the shape diameter function and other mesh information to propose an adaptive MAT generation method which can output a structurally complete initial MAT even for a shape containing extremely thin parts. After mesh conversion, for a dense and redundant initial medial mesh, Q-MAT+ can efficiently simplify it to get a structurally simple, geometrically accurate, and compact MAT representation even with a user-specified Hausdorff error threshold, which is more reasonable than a fixed vertex number. Since Q-MAT+ is feature sensitive, it can preserve significant tubular features during the simplification.

However, our current Q-MAT+ is still unable to preserve sharp features very well on some 3D shapes, such as sharp edges and corners of CAD models, since it involves three difficult aspects: 1) automatic accurate detection of sharp features; 2) the use of spheres (of zero radii) to fit sharp feature; and 3) building up the relationship between the features and MAT. We will continue to investigate these aspects in our future work. Applying MAT as an underlying shape descriptor for more applications, such as 3D animation, object segmentation and classification, is also our future plan.

6. Acknowledgements

We would like to thank Feng Sun for sharing the source code of HEM, and the anonymous reviewers for valuable suggestions. This work was supported by the NSFC under Grant 61772301. The models we use in this paper are provided by Chen et al. (2009) and Aim-at-Shape.

References

Amenta, N., Choi, S., Kolluri, R.K., 2001. The power crust, unions of balls, and the medial axis transform. Computational Geometry 19, 127–153.

Attali, D., Montanvert, A., 1996. Modeling noise for a better simplification of skeletons, in: Proceedings of 3rd IEEE International Conference on Image Processing, pp. 13–16 vol.3.

Blum, H., 1967. A transformation for extracting new descriptors of shape. Models for the Perception of Speech and Visual Form , 362–381.

Brandt, J., Algazi, V., 1992. Continuous skeleton computation by Voronoi diagram. CVGIP: Image Understanding 55, 329–338.

Chazal, F., Lieutier, A., 2005. The "λ-medial axis". Graphical Models 67, 304–331.

Chen, X., Golovinskiy, A., Funkhouser, T., 2009. A benchmark for 3D mesh segmentation. ACM Transactions on Graphics (Proc. SIGGRAPH) 28.

Dey, T.K., Zhao, W., 2004. Approximating the medial axis from the Voronoi diagram with a convergence guarantee. Computer-Aided Design 36, 195–202.

Faraj, N., Thiery, J.M., Boubekeur, T., 2013. Progressive medial axis filtration, in: SIGGRAPH Asia 2013 Technical Briefs, ACM, New York, NY, USA. pp. 3:1–3:4.

Garland, M., 1997. Surface simplification using quadric error metrics. In Proceedings of the 24th annual conference on Computer graphics and interactive techniques , 209–216.

Hesselink, W.H., Roerdink, J.B.T.M., 2008. Euclidean skeletons of digital image and volume data in linear time by the integer medial axis transform. IEEE Transactions on Pattern Analysis and Machine Intelligence 30, 2204–2217.

Hu, K., Yan, D., Bommes, D., Alliez, P., Benes, B., 2017. Error-bounded and feature preserving surface remeshing with minimal angle improvement. IEEE Transactions on Visualization and Computer Graphics 23, 2560–2573.

Jalba, A.C., Sobiecki, A., Telea, A.C., 2016. An unified multiscale framework for planar, surface, and curve skeletonization. IEEE Transactions on Pattern Analysis and Machine Intelligence 38, 30–45.

Ju, T., 2004. Robust repair of polygonal models. ACM Transaction on Graphics 23, 888–895.

Lan, L., Yao, J., Huang, P., Guo, X., 2017. Medial-axis-driven shape deformation with volume preservation. The Visual Computer 33, 789–800.

Li, P., Wang, B., Sun, F., Guo, X., Zhang, C., Wang, W., 2015. Q-MAT: Computing medial axis transform by quadratic error minimization. ACM Transaction on Graphics 35, 8:1–8:16.

Miklos, B., Giesen, J., Pauly, M., 2010. Discrete scale axis representations for 3D geometry. ACM Transaction on Graphics 29, 101:1–101:10.

Palgyi, K., Kuba, A., 1999. A parallel 3D 12-subiteration thinning algorithm. Graphical Models and Image Processing 61, 199–221.

Pizer, S.M., Siddiqi, K., Székely, G., Damon, J.N., Zucker, S.W., 2003. Multiscale medial loci and their properties. International Journal of Computer Vision 55, 155–179.

Pudney, C., 1998. Distance-ordered homotopic thinning: A skeletonization algorithm for 3D digital images. Computer Vision and Image Understanding 72, 404 – 413.

Rumpf, M., Telea, A., 2002. A continuous skeletonization method based on level sets, in: Proceedings of the Symposium on Data Visualisation 2002, Eurographics Association, Aire-la-Ville, Switzerland, Switzerland. pp. 151–ff.

Saha, P.K., Borgefors, G., di Baja, G.S., 2016. A survey on skeletonization algorithms and their applications. Pattern Recognition Letters 76, 3 – 12. Special Issue on Skeletonization and its Application.

Shapira, L., Shamir, A., Cohen-Or, D., 2007. Consistent mesh partitioning and skeletonisation using the shape diameter function. The Visual Computer 24, 249–259.

Sobiecki, A., Jalba, A., Telea, A., 2014. Comparison of curve and surface skeletonization methods for voxel shapes. Pattern Recognition Letters 47, 147 – 156. Advances in Mathematical Morphology.

Sun, F., Choi, Y., Yu, Y., Wang, W., 2016. Medial meshes a compact and accurate representation of medial axis transform. IEEE Transactions on Visualization and Computer Graphics 22, 1278–1290.

Thiery, J.M., Guy, E., Boubekeur, T., 2013. Sphere-meshes: Shape approximation using spherical quadric error metrics. ACM Transaction on Graphics (Proc. SIGGRAPH Asia 2013) 32, Art. No. 178.

Tournois, J., Alliez, P., Devillers, O., 2010. 2D centroidal voronoi tessellations with constraints. Numerical Mathematics: Theory, Methods and Applications 3.

Tsao, Y., Fu, K., 1981. A parallel thinning algorithm for 3-D pictures. Computer Graphics and Image Processing 17, 315 – 331.

Yan, Y., Letscher, D., Ju, T., 2018. Voxel cores: Efficient, robust, and provably good approximation of 3D medial axes. ACM Transaction on Graphics 37, 44:1–44:13.

Yan, Y., Sykes, K., Chambers, E., Letscher, D., Ju, T., 2016. Erosion thickness on medial axes of 3D shapes. ACM Transaction on Graphics 35, 38:1–38:12.

Yang, B., Yao, J., Guo, X., 2018. DMAT: Deformable medial axis transform for animated mesh approximation. Computer Graphics Forum 37, 301–311.